Minimally Invasive Multimodal Flexible Sensors to Monitor Stem Growth Rate, Soil Water Content, And Soil pH

Masaki Teramoto, Lin Shi, Naruhito Seimiya, Kuniharu Takei*

Graduate School of Information Science and Technology, Hokkaido University, Sapporo 060-0814, Japan

*Corresponding author: takei@ist.hokudai.ac.jp

Keywords: multimodal sensor, plant, stem growth rate sensor, soil water sensor, soil pH sensor

Abstract:

Smart agriculture, which integrates sensing, robotics, and AI technologies, offers a promising paradigm to optimize plant growth and resource efficiency. However, current biological monitoring systems are often bulky, invasive, or require multiple discrete devices, which limits their applicability during early-stage plant growth. This study proposes a fully integrated, multimodal flexible sensor system capable of minimally invasive and continuous monitoring of key physiological and environmental parameters, i.e., stem growth rate, soil moisture, and soil pH. A kirigami-structured ultraflexible strain sensor is directly attached to the plant stem to monitor elongation with minimal mechanical interference, achieving the Young's modulus of 5.2 kPa and a strain range up to 340%. An impedance-based soil water sensor inserted into the soil exhibited a sensitivity of 8.1 %/% within the 20-30% soil water content range. A polyaniline-based electrochemical pH sensor embedded in the soil showed a sensitivity of 49.2 mV/pH, determined from potentials immediately after irrigation events. Unlike conventional approaches,

the proposed system realizes accurate, real-time monitoring even during the most sensitive stages of plant development. Notably, the system achieved continuous simultaneous monitoring of all parameters over 80 hours under realistic conditions in a controlled growth chamber. The simultaneous acquisition of stem-based growth metrics and soil environmental data allows for a comprehensive understanding of plant physiology and supports precision agriculture. This work provides a scalable and minimally invasive platform for next-generation ecosystem-driven plant monitoring, thereby paving the way for data-informed, energy-efficient crop management strategies in sustainable agriculture.

Food security is an important issue in the global sustainability context. With accelerating demographic expansion, the intensification of climate-related disruptions and escalating geopolitical tensions have aggravated the food crisis, particularly in vulnerable and resource-constrained nations.[1–3] Enhancing plant yield and promoting efficient growth over a reduced cultivation period are critical in terms of establishing sustainable ecosystems that support highly efficient photosynthesis and consistent vegetable production while minimizing external energy inputs. In this context, smart agriculture, which integrates cutting-edge technologies, e.g., sensors, robotics, and artificial intelligence (AI), has emerged as a transformative paradigm to substantially improve agricultural productivity and environmental sustainability by optimizing resource utilization and crop management strategies.[4–6]

Plant growth is highly dependent on environmental conditions and weather, resulting in the need for a comprehensive understanding of plant biology. Because of importance for sustainable and ecosystem platform based on plants, plant biological studies have become increasingly important,[7] and research has been conducted using several sensors to monitor plant conditions from seed to growth, including growth rate, soil, and transpiration.[8-10] However, most biological tests rely on bulky and expensive sensor systems, and different sensor systems must be prepared to monitor each condition.

A potential alternative is to employ a multimodal flexible sensor system, in which the mechanical flexibility does not affect the growth of the plant. In addition, the integration of multiple sensors reduces device costs and facilitates the measurement of several plant conditions simultaneously without using requiring bulky systems. Recent reviews have summarized advances in the development of multimodal flexible sensors for applications such as wearable devices, robotics, and environment monitoring,[11,12] and these technologies can also be extended to the physiological and condition monitoring of plants. In fact, several flexible sensors to monitor plant conditions have been reported.[8,10] Among the different plant conditions, the stem growth rate is an important factor, and Borode et al. proposed a flexible stem growth monitoring method that employs a stretchable elastomer–based strain sensor to monitor the stem growth rate in real time.[13] However, a systematic study on the impact on plant growth caused by the relatively large Young's modulus of the elastomer has not been conducted. The stem growth rate is a key quantitative indicator of overall plant health, and early-stage stem growth is particularly sensitive to various factors, e.g., irrigation volume and soil nutrient availability.[14] Thus, the stem growth rate must be monitored to improve crop yields and promote healthy plant development. However, early-stage stems exhibit rapid elongation, requiring sensors with a wide strain sensing range, and due to their slender geometry, sensor-induced mechanical stress could impede growth. Thus, realizing long-term, accurate stem growth monitoring remains a challenge.

A previous study monitored the continuous transpiration on a leaf, environmental temperature, humidity, and light exposure simultaneously by integrating each sensor on a flexible film.[15–25] In addition, other studies have reported the use of leaf deformation as an indicator of growth.[13,15,26,27] However, leaves are subject to different physiological processes, e.g., photosynthesis, transpiration, and leaf temperature fluctuations, and these factors may interfere with accurate growth assessment.[10] Thus, from the perspective of evaluating plant growth precisely, stem-based monitoring is considered more effective than leaf-based approaches. Furthermore, several approaches have demonstrated strain sensors for monitoring the circumference growth of fruits.[28-31] Lo Presti et al. also developed an optical strain sensor to measure dimensional changes in both leaves and fruits.[32] Although sensors for fruit monitoring can effectively track localized dimensional changes, fruit-based monitoring methods may not be directly applicable to stems due to distinct sensor conformability and mechanical constraints.

Various plant monitoring applications have been demonstrated; however, effective monitoring of soil information with stem growth rate, which are both key parameters relative to enhancing plant growth, has not been demonstrated using an integrated flexible sensor system with a stem growth sensor. While soil monitoring enables indirect assessment of plant health, growth measurements provide a more direct and intrinsic indicator of a plant's physiological status. Thus, the simultaneous monitoring of both factors is expected to facilitate the comprehensive study of plant physiology.

To advance plant physiological studies, this study proposes an integrated multimodal flexible sensor that can monitor the stem growth rate, soil water content, and soil pH continuously and minimal invasively. Here, for the stem growth rate, a flexible strain sensor is attached to the stem of the plant. In the early stages of plant growth, the stem is thin; thus, it is important to ensure that the monitoring process does not hinder growth. To prevent growth from being impeded due to attaching the sensor, a strain sensor with high softness is realized by utilizing a kirigami structure in a film. In addition, a pair of electrodes is formed on a film to measure the impedance through the soil and water for water content, and the pH of the water in the soil is evaluated using an electrochemical reaction of polyaniline (PANI). These water content and pH sensors are installed in the soil, whereas the strain sensor is positioned on the stem of the plant. In this study, all sensors were first characterized separately, and then they were integrated as a multimodal flexible sensor sheet by optimizing the sensor fabrication and integration processes. The sensor sheet was connected to a wireless module to enable real-time data visualization on a smartphone device. Finally, simultaneous monitoring of all information is demonstrated as a proof-of-concept for plant applications. The proposed method enables the simultaneous monitoring of plant growth and soil conditions, and the findings of this study are expected to contribute to data-driven and sustainable smart agriculture. The key advantage of this work lies in the combination of a highly soft kirigami-structured strain sensor for minimally invasive stem growth monitoring and integrated soil sensors. To the best of our knowledge, this is the first demonstration of an integrated multimodal flexible sensor system capable of simultaneously monitoring stem growth and multiple soil parameters in real time.

Results and Discussion

A multimodal sensor sheet was fabricated to enable real-time, comprehensive monitoring of plant growth and soil conditions (Figure 1a). The sensor sheet integrates a strain sensor, a soil water sensor, and a soil pH sensor on a 25 μm-thick polyethylene terephthalate (PET) film (Figure 1b) based on the fabrication process illustrated in Figure S1. The process is described in detail in the Method section. The strain sensor incorporates a kirigami structure, which provides exceptional mechanical flexibility and stretchability[33–36] that enables minimally invasive monitoring of early-stage stem growth. The soil water sensor, comprising a pair of electrodes, is inserted into the soil to estimate the water content by measuring the impedance change, contributing to irrigation optimization efforts and water resource conservation. The soil pH sensor continuously monitors the acidity of the water in the soil to help ensure an optimal pH environment for crop growth while mitigating soil and water pollution resulting from the excessive use of fertilizers.

Flexible stem growth rate (strain) sensor

A highly flexible sensor design is required to enable strain sensing of the early-stage stem growth without interfering with the plant's growth. The fabrication process of the strain sensor is shown in Figure S2. Here, a kirigami structure was introduced to reduce mechanical stiffness while maintaining sufficient stretchability (Figure 2a). As a baseline configuration, the sensing material comprised carbon black (CB) with polydimethylsiloxane (PDMS) and an Ecoflex mixture. The thickness of the sensing layer was approximately 84 μm. The sensing mechanism relies on monitoring the resistance change, which reflects changes in the contact area between the CB particles during stretching in the PDMS/Ecoflex (Figure 2b). As shown in Figure 2c, the kirigami structure reduces the stress caused by the strain by approximately 11 times compared to that without the kirigami structure due to the structural deformation of the kirigami. Quantitatively, the Young's modulus extracted from the results shown in Figure 2c exhibited a significant reduction from 320 kPa with the non-kirigami structure to 5.2 kPa with the kirigami structure.

In terms of structural optimization, four kirigami patterns were designed and characterized (Figure S3a). Mechanical tests of the stress-strain curves demonstrated that increasing the slit width from 0.1 mm to 0.5 mm improved the maximum strain considerably, while increasing the length of the line from 2 mm to 2.3 mm slightly reduced the tensile stress and improved the stretchability (Figure S3b). Although the stretchability is limited for pattern A (length: 2 mm; width 0.1 mm), as a strain sensor, the resistance change ratio as a function of strain (Figure S3c) was the best among all patterns. Based on the balance between flexibility and the resistance change ratio with stable measurements, pattern A was selected.

The effect of the PDMS/Ecoflex composition ratio was also characterized to enhance the mechanical and sensing properties. Here, a higher Ecoflex content resulted in greater stretchability (Figure 2d) and lower Young's modulus values (Figure 2e), which is consistent with the material properties, in which Ecoflex is softer than PDMS. Under repeated stretching cycles, the resistance change ratio $\Delta R/R_0$, where ΔR denotes the resistance change from the initial resistance value R_0 without strain, showed relatively stable responses for all compositions, despite the presence of hysteresis (Figure S4a). The initial-cycle sensitivity in the 0–50% strain range was 1.11–1.78%/% (resistance change ratio per strain)(Figure S4b), and the sensors with higher Ecoflex content exhibited a wider strain sensing range (Figure S4c). Notably, the gauge factor reached a maximum at the 1:1 composition ratio of PDMS and Ecoflex in both the 0–50% and 50–100% strain ranges, as shown in Figure S4d. Although the mechanism underlying this behavior remains unclear, it is hypothesized that an intermediate ratio of PDMS and Ecoflex may create a composite structure in which strain is more effectively transferred to the conductive CB network, resulting in a larger resistance change. Further microscopic analysis would be needed to elucidate this phenomenon in detail.

This sensor system is designed to monitor plant conditions; thus, the temperature dependence of the sensor is an important factor in terms of realizing stable monitoring. To reduce the temperature effect on the strain sensor, which frequently has a large temperature dependence due to the thermal expansion of elastomer materials,[37] the composition of the Ecoflex in the PDMS was investigated. The resistance change ratio at different composition ratios of Ecoflex was measured using an environmental oven from 20–55°C. Higher temperatures increase the resistance for all composition ratios due to fewer CB particle contacts caused by the thermal expansion of the elastomer (Figure 2f). Interestingly, although the Ecoflex has a higher thermal expansion coefficient than PDMS,[38] the sensors with higher Ecoflex content demonstrated lower resistance change ratios. This discrepancy may be attributed to nonuniform deformation due to the mixture of Ecoflex and PDMS or differences in the chemical bonding. However, this is speculation, and this phenomenon should be investigated more extensively in the future, which is beyond the scope of the current study. Based on these results, Ecoflex without PDMS exhibited the lowest influence on the temperature change. However, the Ecoflex with CB has excessive adhesion on the handling substrate in the fabrication process, which resulted in a low fabrication yield. Considering the flexibility, sensing range, thermal stability, and processability, a PDMS/Ecoflex ratio of 1:3 was selected in this study.

The CB content was then optimized to improve the mechanical and sensing performance. The tensile test showed that increasing the CB content improved both the tensile strength and Young's modulus (Figures S5a and S5b). The 3% CB sensor did not have initial conduction; thus, this sensor configuration was excluded from the sensor response tests. The 5%, 7%, and 9% CB sensors exhibited stable resistance change ratios over multiple cycles despite the presence of hysteresis (Figure S5c). A lower CB content resulted in higher sensitivity (Figure S5d) due to the sparse conductive network.[39,40] Sensors with higher CB content demonstrated more stretchability and resistance change stability without fluctuation at high strain (Figure S5e). In terms of the temperature effect relative to the CB content, there was no significant difference in the range of 15°C to 40°C (Figure S5f). Based on the performances about stretchability, softness, and sensitivity as a strain sensor to monitor early stage stem growth, 7 % CB content was used in this study.

The effect of the sensor thickness (i.e. PDMS/Ecoflex/CB composite film) was also evaluated. Thicker films exhibited lower stretchability and required higher force at failure (Figures S6a and S6b). Regardless of the thickness, all sensors exhibited stable responses during repeated stretching (Figure S6c), and thinner films had lower sensitivity due to the lower stress in the film based on strain engineering (Figure S6d). Similar to the results of the CB content change in the PDMS/Ecoflex, the temperature coefficient between 15°C and 50°C was nearly the same as that observed in the range of 0.27%/°C to 0.31%/°C with no significant variation across the different thicknesses (Figure S6e). To minimize the mechanical stress on the stems during growth monitoring, the 84-μm film thickness, which required the lowest force at the maximum strain, was selected in this study. Although a 69 μm-thick film was also fabricated, it was excluded from further analysis due to poor fabrication reproducibility caused by its thinness.

After optimizing all of the material and design parameters, the electrical responses were characterized as a plant-based strain sensor. First, the resistance change ratio was measured as a function of the stretching tensile strain until broken (Figure 2g). Here, the strain sensing range reached up to 340%, and the sensitivities extracted by linear fitting were 0.27 %/% ($0 < \varepsilon < 90\%$), 2.84 %/% ($90\% < \varepsilon < 270\%$), and 14.4 %/% ($270\% < \varepsilon < 340\%$). Then, the humidity dependence was evaluated using an environmental oven to control the humidity at 25°C. As shown in Figure 2h, the resistance change ratios remained below 0.5% across a relative humidity range of 35% to 95% with a slightly increasing trend with increasing humidity. The resistance change caused by the strain was much greater than that caused by the humidity change; this small variation is negligible. Therefore, this strain sensor can be used to perform stable measurements of the growth rate regardless of any changes in the environmental humidity.

A key challenge to address in this study is to monitor stem growth using a strain sensor without affecting the growth of the plant. To confirm the effect of attaching the sensor to the plant, a comparative test was performed using young soybean stems with and without sensors (Figure 2i). Strain sensors were fixed to stems by attaching polyimide (PI) tape to the Ag electrode regions at both ends of the sensors and gently wrapping the tape around the stems. Although individual variations were observed, the difference in the average stem growth rate was only 1.3% (N=6 for each condition), which suggests that attaching the sensor for growth rate monitoring has a negligible impact on plant growth.

The feasibility of real-time plant monitoring using the developed strain sensor was investigated (Figures 2j and S7). The sensor was attached close to the growth point of the stem to enable growth over a longer period. Note that due to the drift of the sensor outputs, which was observed to be repeatable, the sensor output used to calculate the length change ratio $\Delta L/L_0$, where ΔL denotes the stem length change from the initial length L_0, was calibrated to remove the effect of the drift (Figures S8a and S8b). Specifically, to standardize the initial resistance change ratio at the start of measurement and to compensate for the drift, the sensor was subjected to a 100% strain stretching cycle prior to attachment to the stems. The resistance change ratio obtained from the sensor outputs was calibrated by adding the resistance change ratio corresponding to the time-dependent decrease. The environmental conditions during the test were maintained at 20°C to 25°C and 20% to 25% humidity (Figures S8c and S8d). As a control to confirm the accuracy of the sensor output, the growth rate was also measured using a camera (Figure S8e). Here, the growth rate and trend were well matched between the strain sensor and the camera monitoring, which indicates that the strain sensor can be used to monitor the stem growth rate in real time. It is worth to note that temporary reductions in growth were observed. This was caused by the fact that the stem growth is not perfectly linear and involves irregular movement, as revealed by the time-lapse images shown in Figure S8e, and this irregular movement during growth occasionally released strain in the sensor.

Based on these properties, a comparison of the strain sensors developed in previous studies for plant growth monitoring is shown in Table S1.[13,15,22,26-32] Most sensors reported previously were not evaluated in terms of their performance under different environmental factors, e.g., temperature and humidity, which were investigated systematically in this study. In addition, the strain sensor developed in this study leverages the kirigami structure to achieve exceptional flexibility, which enables minimally invasive monitoring of early-stage stem growth. This design surpasses the performance reported in previous studies, offering a more effective solution for plant growth monitoring.

Soil water (impedance) sensor

Efficient soil water management is essential for healthy crop growth.[41,42] To facilitate soil water management, an impedance-based soil water sensor using CB electrodes was developed (Figure 3a). This sensor comprises Ag and CB electrodes printed onto a PET film, with an acrylic plate attached to the backside of the CB electrode to provide structural support when it is inserted into the soil (Figure 3b). The detailed fabrication process is explained in the Method section and Figure S9. The sensor operates by inserting the electrodes into the soil and applying an alternating current voltage to measure the impedance between the CB electrodes via the soil. The impedance value was calculated to extract the water content.

First, the effect of the CB electrode distance was characterized by calculating the sensitivity to the water content. The sensitivity was calculated by linear fitting of the impedance change ratio, $\Delta Z/Z_0$, where ΔZ is impedance difference from the initial impedance Z_0 at 12% water content at 1 kHz, as a function of the water content between 12% and 26% in the soil (Figure S10). Figure 3c indicates that the sensitivity increases as the electrode distance increases. The sensor with a 2-mm electrode distance exhibited almost no sensitivity at low water content, likely due to the insufficient path length through the soil and water, coupled with the relatively large soil particle diameter (~1.0 mm). In contrast, increasing the electrode distance clearly enhanced the sensitivity, showing a distinct trend of decreasing impedance as the water content increased. Most likely, by increasing the electrode distance more than 5 mm, sensor sensitivity may be improved further. However, by considering the sensor size in soil, a 5-mm electrode distance was selected.

Next, the frequency dependence of the impedance in the soil was studied with different water content (Figure 3d). Above ~30 kHz, the impedance curves exhibited minimal differentiation across varying water levels, whereas a clear divergence in impedance was observed at frequencies below 30 kHz, corresponding to different water content levels. Furthermore, a larger impedance change was observed at lower frequencies. However, at lower frequency, impedance fluctuation became large. By considering the important soil water content range of approximately 20%–30%, the need for stable monitoring with less noise, and the clear phase difference (Figure S11), the measurement frequency of 1 kHz was selected.

At the optimal measurement frequency of 1 kHz, the correlation between the soil water content and the impedance change was evaluated using the developed water sensor with the water content measured by the commercial sensor (Figure 3e). Within the linear range of 12% to 20% water content, the sensitivity was relatively low at 0.39%/%. However, since this range corresponds to dry soil conditions where irrigation is typically required, the practical impact of this limitation is minimal. In the critical water content range for plant growth (~20–30%), the sensor demonstrated a high average sensitivity of 8.1%/%, highlighting its suitability for precise water monitoring. Although sensitivity slightly decreased beyond 30% water content, the impact was minimal as irrigation was generally lower in this range.

Since soil temperature varies under environmental conditions, it is necessary to evaluate the impact of temperature on the impedance measurements. The sensor was immersed in phosphate-buffered saline (PBS), and the solution temperature was varied from 20°C to 50°C. As the temperature increased, the impedance gradually decreased, but the maximum rate of change remained below 0.8% (Figure 3f). Compared to the impedance change induced by the soil water variation, this temperature-induced variation was minimal, indicating that the temperature effects were negligible. Impedance can also be affected by ionic concentration, such as dissolved salts and nutrients, which will be the focus of a future study to integrate with ionic sensor to distinguish the effects of water content and ionic conductivity for more accurate monitoring.

Although, in this study, the sensor is intended for use without bending to inset the sensor in soil easily, its mechanical tolerance was evaluated by attaching it to curved surfaces and measuring in PBS since it can potentially be a flexible impedance sensor (Figure 3g). The impedance variation remained below 0.2%, indicating high stability under bending.

Finally, long-term real-time monitoring of the soil water was conducted over 100 h using both the developed impedance sensor and a commercial soil water sensor (Figure 3h). During this period, five irrigation events were performed. In the water range of ~20–30%, both sensors exhibited consistent responses to water content variations, confirming the high tracking ability and reliability of the developed sensor, and both sensors exhibited consistent responses to water content variations, confirming the high tracking ability and reliability of the developed sensor. The results demonstrate the sensor's effectiveness for efficient water management.

Flexible soil pH sensor

Since soil pH significantly influences nutrient availability and crop growth, real-time monitoring is important to realize sustainable plant growth and agriculture.[42-43] To realize continuous and real-time pH monitoring in the soil, a PANI-based pH sensor was developed (Figure 4a). The sensor consists of a PANI working electrode (WE) and an Ag/AgCl reference electrode (RE). The detailed process is described in the Method section and illustrated in Figure S12. Here, PANI was electrochemically deposited on a CB electrode using chronoamperometry and cyclic voltammetry (Figure S13), and the pH was detected through protonation and deprotonation reactions occurring on the surface of the PANI membrane.[44-46]

The pH sensor was characterized in buffer solutions with varying pH values. Figure 4b shows the time-series potential change at different pH levels. As can be seen, each pH level was detected repeatedly with negligible hysteresis, and the variation between the increasing and decreasing pH measurements was minimal, with only a 2.0% difference, demonstrating stable operation (Figure S14). For soil pH monitoring, the sensor was characterized by embedding it in soil and applying solutions of different pH levels (Figure 4c). Immediately after watering in soil, the output voltage changed sharply and then gradually drifted in the reverse direction. This behavior is attributed to the initial direct contact of the solution with the electrode, followed by gradual absorption into the soil and decreasing water content near the electrode over time. Due to the peak and drift behaviors of the potential on the pH sensor in the soil, the potential corresponding to the pH was extracted from the peak value immediately after applying water. The sensitivities in the solution both directly and in soil were 58.8 mV/pH and 49.2 mV/pH, respectively (Figure 4d). The sensitivity of the sensor in the soil was lower than that in the solution; however, it still exhibited high linearity. The lower sensitivity is likely due to the limited interaction between the PANI surface and the solution because the applied solution was absorbed rapidly by the surrounding soil. Nonetheless, the high linearity confirms sufficient practicality for soil pH monitoring.

To investigate the effect of the amount of water in the soil for pH sensing, tap water (pH 7.2) was added to the soil to adjust the water content, and the output voltage was measured (Figure 4e). Here, the output was normalized to observe the effect of the water content for pH detection, where the outputs at 10% and 30% water were set to 0 and 1, respectively. The output increased with increasing water content and saturated at 1 above 30% water content. Based on the results, the pH value must be calculated depending on the water content.

To further investigate the effect of ionic composition, we measured the output potential after thoroughly mixing the soil with PBS, PBS with an additional 10 mM NaCl, and PBS with an additional 100 mM NaCl to adjust the water content to 40% (Figure S15) while keeping pH value of 7.2. The results showed that the measured potential remained almost the same between PBS and PBS with an additional 10 mM NaCl, while the addition of 100 mM NaCl resulted in approximately a 7 mV potential increase. This trend is consistent with the previous study on PANI-based pH sensors,[47] which have reported potential shifts due to changes in ionic strength. To address this issue, the incorporation of a protective polyvinyl butyral (PVB) coating over the PANI layer or the integration of ion sensors may be required to enable calibration for ionic strength variations.

Generally, pH sensors have temperature dependence based on the Nernst theory. To assess the temperature dependence of the PANI-based pH sensor, the sensor was immersed in a buffer solution of pH 5.1, 6.8, and 8.1, and the output voltage was measured while varying the temperature from 20°C to 40°C (Figure 4f). The output potential decreased with increasing temperature, and the observed sensitivity trend aligned with the theoretical Nernstian response as a function of the measured temperature (Figure S16). The temperature sensitivity was sufficiently small compared with the pH sensitivity; however, to realize sufficiently accurate monitoring, a temperature sensor must be integrated, which will be the focus of future work to realize a more practical sensor system. Although this temperature dependence was evaluated in solution, further studies will be needed to assess the effect of soil temperature variations under realistic conditions.

Since the sensor may experience slight deformation due to soil pressure, its bending tolerance was evaluated (Figure 4g). Under bending with a curvature radius up to 1 cm, the output voltage change remained within ±5 mV. This potential change caused by bending corresponds to a fluctuation of approximately 0.1 pH, which is likely sufficiently low to realize stable monitoring of the pH level in the soil. Notably, after returning the sensor to a flat state, the output gradually recovered and stabilized near the initial value at the flat state (Figure S17).

Accordingly, soil pH monitoring over 100 hours was performed using tap water for irrigation (Figure 4h). Throughout the evaluation period, which included multiple irrigation events, the pH values calculated from the fabricated soil pH sensor closely matched those measured with the commercial pH sensor, particularly immediately after irrigation. Repeated measurements over multiple irrigation cycles demonstrated consistent sensor responses, confirming good stability and reproducibility during prolonged use although an error response was also observed. It should be noted that the commercial pH sensor measured the pH of the water before it was added to the soil rather than directly measuring the soil pH.

To further evaluate the long-term stability of the printed Ag/AgCl electrode, a continuous potential monitoring was conducted between the printed Ag/AgCl and a commercial glass Ag/AgCl electrode in PBS over 100 hours. The initial potential difference was approximately 50 mV (positive on the ink electrode), and a gradual decrease in the potential was observed over time (-0.177 mV/h), with a total drift of approximately 20 mV after 100 hours (Figure S18). However, in this study, the pH sensor was used to monitor the pH of the soil solution after periodic irrigation rather than under continuous immersion conditions. The pH values obtained immediately after irrigation remained consistent with those measured by a commercial pH sensor (Figure S19), indicating that the influence of drift was limited under practical conditions in this study.

Demonstration of integrated sensor system

Finally, a multimodal flexible sensor sheet integrated with a strain sensor, a soil water sensor, and a soil pH sensor was tested in a real-time experiment conducted over more than three days.

The sensor sheet was divided into strain measurement and soil measurement sections, which were attached to the stem and inserted into the soil, respectively (Figure 5a).

The growth monitoring results obtained using the strain sensor showed that growth at the sensor attachment area stopped approximately 48 hours after the measurement began (Figure 5b) because the growth point shifted to the upper part of the stem, thereby causing the growth at the sensor-attached area to stop. The strain sensor tracked the stem growth successfully with high accuracy during the measurement period and maintained relatively stable responses even after the growth stopped. This range of growth monitoring is considered sufficient for the purposes of the current study, which focused on monitoring early-stage growth.

The soil water sensor accurately tracked the changes in the soil water content (Figure 5c). After each irrigation event, the sensor detected a rapid increase in soil moisture, followed by a decrease due to evaporation. However, unlike the commercial sensor, which showed a smooth decline in the soil water content, the fabricated sensor exhibited an irregular decrease, particularly in regions with high water content. This irregularity is likely due to issues specific to the fabricated sensor, e.g., inconsistent contact between the electrodes and the soil. Despite this irregularity, the fabricated sensor responded to changes in the soil water content over multiple irrigation cycles, thereby demonstrating its overall reliability for continuous soil water monitoring.

The pH values calculated from the flexible soil pH sensor closely matched those measured with the commercial pH sensor, particularly immediately after irrigation (Figure 5d). This result is consistent with the results obtained from the single pH sensor demonstration, confirming the measurement accuracy of soil solution pH.

Longer-term growth monitoring could be possible by detaching the sensor and reattaching it near the shifted growth point if the growth point moves and the sensor no longer detects growth changes; however, this was not investigated in this evaluation. In terms of the soil pH monitoring, the relationship between the soil water content and the potential of the pH sensor (Figure 4e) suggests that it may be possible to estimate the soil pH immediately after water is added and during other periods. However, the soil was not stirred in this demonstration; thus, the nonuniform distribution of the soil water made the continuous pH measurement difficult. Therefore, developing a system that can continuously monitor the soil pH using the relationship between the soil water content and the potential difference of the pH sensor, even without stirring the soil, remains an ongoing challenge.

Additional measurements using the multimodal sensor system demonstrated consistent sensor responses and confirmed its reproducibility (Figure S20). During the demonstration, the soil-embedded water content sensor and pH sensor were able to independently and simultaneously measure their respective parameters without abnormal fluctuations, indicating that no signal interference occurred under the tested conditions.

Conclusion

In this study, we developed a multimodal sensor sheet for comprehensive, real-time monitoring of plant growth and soil conditions toward the realization of precision agriculture and sustainable crop management. The proposed sensor sheet integrates three flexible sensors, i.e., a kirigami-structured strain sensor, a CB-based soil water sensor, and a PANI-based soil pH sensor, onto a PET film. Each sensor was fabricated and characterized. The strain sensor exhibited high stretchability and flexibility, enabling minimally invasive monitoring of early-stage stem growth. The soil water sensor demonstrated stable impedance responses with optimized electrode spacing and operating frequency, achieving high sensitivity in the 20% to 30% water range, which is important for plant growth. In addition, the soil pH sensor demonstrated reliable responses in both solution and soil environments, with high linearity and stability under varying temperature and bending conditions. Finally, simultaneous real-time monitoring of plant growth and soil conditions using the proposed sensor-integrated multimodal sensor sheet was demonstrated, and the consistent performance of each sensor in the integrated system highlights the feasibility of applying this approach in smart agriculture applications.

The remaining challenges include improving the long-term stability of the system under various environmental conditions and evaluating plant growth under different soil water content levels and pH levels. In addition, practical evaluations in large-scale agricultural environments will be required to realize real-world applications. Although these challenges should be addressed in future studies, the stable and minimally invasive integrated flexible sensor system proposed in this study represents a significant step toward in the development of advanced plant monitoring technologies.

Methods

Device Fabrication

Integrated Sensor: The process used to fabricate the integrated sensor is illustrated in Figure S1. First, the Ag electrodes were printed on 25 μm-thick PET film (Figure S1(1)). Next, the film with the Ag electrodes was laminated with a 25 μm-thick PET film, followed by cutting the square film for strain sensing (Figure S1(2)). The impedance sensor was then fabricated by printing the CB electrodes (Figure S1(3)). Subsequently, the strain sensor module was attached to the Ag electrodes (Figure S1(4)), followed by formation of the pH sensor (Figure S1(5)). Finally, the unnecessary areas of the film were removed (Figure S1(6)). The fabrication process of each sensor is described in the following.

Strain Sensor: The PDMS (SILPOT 184) base and curing agent were mixed at a weight ratio of 10:1, and the Ecoflex (Ecoflex 00-30) base and curing agent were mixed at 1:1. The two mixed solutions were then combined at a predetermined PDMS/Ecoflex weight ratio, followed by the addition of CB powder (acetylene, ≥99.9%, Wako, Japan) as a conductive filler. The composite solution was stirred at 1500 rpm for 3 min (Figure S2(1)). The composite was blade-coated onto a PET film and cured at 90°C for 30 min (Figure S2(2)). An Ecoflex insulating layer was then applied on the top surface of the PDMS/Ecoflex/CB film as a protective layer against contact with the plant stem (Figure S2(3)). After curing the Ecoflex at 90°C for 5 min, the sensor film was peeled off from the PET film, and a kirigami pattern was introduced using a laser cutter tool (Figure S2(4)). Finally, the Ag electrodes were printed on both ends of the conductive film (Figure S2(5)).

Soil water Sensor: The Ag electrodes were screen-printed onto a 25 μm-thick PET film and cured at 70°C for 5 min (Figure S10(1)). The CB electrodes were printed using CB ink (RA FS 090 S, Toyo Ink, Japan) on the Ag electrodes using a dispensing machine and then cured at 70°C for 10 min (Figure S10(2)). A PET passivation film was laminated over the Ag electrodes, except for the CB electrode area (Figure S10(3)). An acrylic plate (thickness: 1 mm) was then attached to the opposite side of the CB electrodes (Figure S10(4)). Finally, the PET and acrylic plates were patterned by a laser cutter to form a defined sensing gap (Figure S10(5)).

pH Sensor: The Ag electrodes were screen-printed onto a 25 μm-thick PET film and cured at 70°C for 5 min (Figure S13(i-1)). A CB electrode was printed using CB ink on the Ag electrode using a dispensing machine and then cured at 70°C for 15 min (Figure S13(i-2)). PI films were laminated over the Ag electrodes as a passivation layer (Figure S13(i-3)), and the PANI layer was formed by the electrodeposition method[47] on the CB electrode (Figure S13(i-4)). The seeding layer was nucleated at 0.8 V for 60 s in a solution of 0.1 M aniline and 0.1 M HCl using the chronoamperometry method. Subsequently, PANI was deposited via cyclic voltammetry at a scan rate of 100 mV/s in the potential range of −0.2 V to 0.8 V for 25 cycles. The Ag/AgCl ink (ALS, Japan) was printed on the Ag electrode and cured at 70°C for 5 min to form the Ag/AgCl reference electrode (Figure S13(ii)).

Plant Growth: Soybean seeds and soil were purchased from Atariya Farm and Tachikawa Heiwa Farm, Japan, respectively. The real-time measurement of stem growth, soil water content, soil pH was performed in a growth chamber. The temperature was maintained between 20°C and 25 °C using a thermostat and a panel heater. A commercial LED panel (wavelength range: 450–660 nm) was used as the light source and was turned on daily from 09:00 to 21:00. Approximately 20 mL of tap water was applied at a fixed time when the soil surface was visually confirmed to be dry.

Real-time Plant Growth Monitoring: For the real-time measurement, the strain sensing and soil water sensing units were connected to a wireless Bluetooth low-energy circuit, and the pH sensing unit was connected to a data logger (Hioki, LR8400). The soil water and soil pH sensors were placed in the soil 3 cm from the plant to avoid potential interference with root growth.

Supporting Information

The Supporting Information is available free of charge at…

- Details of experimental section; fabrication processes for each sensor and integrated sensor sheet; mechanical properties and electrical characteristics of strain sensor at different material compositions; growth measurement of a plant stem; strain sensor calibration; impedance change at different electrode distances; phase characteristics of the water sensor; chronoamperometry of the PANI seed layer for the pH sensor; Hysteresis of the pH sensor response; ion effect, temperature sensitivity, recovery time characteristic, and reproducibility of the pH sensor; Potential drift of the Ag/AgCl electrode; Real-time monitoring of multiple plant conditions.
- Table for comparison of strain sensor performance for plant growth monitoring.

Conflict of Interest

The authors declare no conflict of interest.

Author Information

Corresponding Author

Kuniharu Takei – Graduate School of Information Science and Technology, Hokkaido University, Sapporo, Hokkaido 060-0814, Japan. https://orcid.org/0000-0001-9166-3747

Authors

Masaki Teramoto - Graduate School of Information Science and Technology, Hokkaido University, Sapporo, Hokkaido 060-0814, Japan.

Lin Shi - Graduate School of Information Science and Technology, Hokkaido University, Sapporo, Hokkaido 060-0814, Japan.

Naruhito Seimiya - Graduate School of Information Science and Technology, Hokkaido University, Sapporo, Hokkaido 060-0814, Japan.

Acknowledgements

This work was partially supported by JST ALCA-Next (No. JPMJAN23F1), JSPS KAKENHI (Grant No. JP22H00594, JP24H00887), JST ASPIRE for Rising Scientists (JPMJAP2336), and the Murata Science Foundation.

References

(1) Molotoks, A.; Smith, P.; Dawson, T. P. Impacts of land use, population, and climate change on global food security. *Food Energy Secur.* **2020**, *10* (1), e261.

(2) Pawlak, K.; Kołodziejczak, M. The Role of Agriculture in Ensuring Food Security in Developing Countries: Considerations in the Context of the Problem of Sustainable Food Production. *Sustainability* **2020**, *12* (13), 5488.

(3) Mavroeidis, A.; Roussis, I.; Kakabouki, I. The Role of Alternative Crops in an Upcoming Global Food Crisis: A Concise Review. *Foods* **2022**, *11* (22), 3584.

(4) Quy, V. K.; Hau, N. V.; Anh, D. V.; Quy, N. M.; Ban, N. T.; Lanza, S.; Randazzo, G.; Muzirafuti, A. IoT-Enabled Smart Agriculture: Architecture, Applications, and Challenges. *Appl. Sci.* **2022**, *12* (7), 3396.

(5) Rajak, P.; Ganguly, A.; Adhikary, S.; Bhattacharya, S. Internet of Things and smart sensors in agriculture: Scopes and challenges. *J. Agric. Food Res.* **2023**, *14*, 100776.

(6) Kumar Kasera, R.; Gour, S.; Acharjee, T. A comprehensive survey on IoT and AI based applications in different pre-harvest, during-harvest and post-harvest activities of smart agriculture. *Comput. Electron. Agric.* **2024**, *216*, 108522.

(7) Henkhaus, N.; Bartlett, M.; Gang, D.; Grumet, R.; Jordon-Thaden, I.; Lorence, A.; Lyons, E.; Miller, S.; Murray, S.; Nelson, A.; et al. Plant science decadal vision 2020-2030: Reimagining the potential of plants for a healthy and sustainable future. *Plant Direct* **2020**, *4* (8), e00252.

(8) Lee, G.; Wei, Q.; Zhu, Y. Emerging Wearable Sensors for Plant Health Monitoring. *Adv. Funct. Mater.* **2021**, *31* (52), 2106475.

(9) Yin, H.; Cao, Y.; Marelli, B.; Zeng, X.; Mason, A. J.; Cao, C. Soil Sensors and Plant Wearables for Smart and Precision Agriculture. *Adv. Mater.* **2021**, *33* (20), e2007764.

(10) Lo Presti, D.; Di Tocco, J.; Massaroni, C.; Cimini, S.; De Gara, L.; Singh, S.; Raucci, A.; Manganiello, G.; Woo, S. L.; Schena, E.; et al. Current understanding, challenges and perspective on portable systems applied to plant monitoring and precision agriculture. *Biosens. Bioelectron.* **2023**, *222*, 115005.

(11) Hou, Y.; Xu, Y.; Cai, Z.; Wu, H.; Li, Y.; Shen, Z.; Xie, H.; Xu, K. Decoupled approaches for multimodal flexible sensor systems. *Nano Res.* **2025**, DOI: 10.26599/NR.2025.94907673

(12) Xu, K.; Cai, Z.; Luo, H.; Lu, Y.; Ding, C.; Yang, G.; Wang, L.; Kuang, C.; Liu, J.; Yang, H. Toward Integrated Multifunctional Laser-Induced Graphene-Based Skin-Like Flexible Sensor Systems. *ACS Nano* **2024**, *18* (39), 26435-26476.

(13) Borode, T.; Wang, D.; Prasad, A. Polyaniline-based sensor for real-time plant growth monitoring. *Sens. Actuators. A Phys.* **2023**, *355*,114319.

(14) Roy, M.; Mathew, F. M.; Prasad, A. Biomechanics of vascular plant as template for engineering design. *Materialia* **2020**, *12*, 100747.

(15) Nassar, J. M.; Khan, S. M.; Villalva, D. R.; Nour, M. M.; Almuslem, A. S.; Hussain, M. M. Compliant plant wearables for localized microclimate and plant growth monitoring. *npj Flex. Electron.* **2018**, *2* (1), 24.

(16) Someya, D.; Arai, S.; Fujie, T.; Takeoka, S. Extracellular pH imaging of a plant leaf with a polyelectrolyte multilayered nanosheet. *RSC Adv.* **2018**, *8* (62), 35651-35657.

(17) Zhao, Y.; Gao, S.; Zhu, J.; Li, J.; Xu, H.; Xu, K.; Cheng, H.; Huang, X. Multifunctional Stretchable Sensors for Continuous Monitoring of Long-Term Leaf Physiology and Microclimate. *ACS Omega* **2019**, *4* (5), 9522-9530.

(18) Lan, L.; Le, X.; Dong, H.; Xie, J.; Ying, Y.; Ping, J. One-step and large-scale fabrication of flexible and wearable humidity sensor based on laser-induced graphene for real-time tracking of plant transpiration at bio-interface. *Biosens. Bioelectron.* **2020**, *165*, 112360.

(19) Lu, Y.; Xu, K.; Zhang, L.; Deguchi, M.; Shishido, H.; Arie, T.; Pan, R.; Hayashi, A.; Shen, L.; Akita, S.; et al. Multimodal Plant Healthcare Flexible Sensor System. *ACS Nano* **2020**, *14* (9), 10966-10975.

(20) Chai, Y.; Chen, C.; Luo, X.; Zhan, S.; Kim, J.; Luo, J.; Wang, X.; Hu, Z.; Ying, Y.; Liu, X. Cohabiting Plant-Wearable Sensor In Situ Monitors Water Transport in Plant. *Adv. Sci.* **2021**, *8* (10), 2003642.

(21) Fiorello, I.; Meder, F.; Mondini, A.; Sinibaldi, E.; Filippeschi, C.; Tricinci, O.; Mazzolai, B. Plant-like hooked miniature machines for on-leaf sensing and delivery. *Commun. Mater.* **2021**, *2* (1), 103.

(22) Hsu, H. H.; Zhang, X.; Xu, K.; Wang, Y.; Wang, Q.; Luo, G.; Xing, M.; Zhong, W. Self-powered and plant-wearable hydrogel as LED power supply and sensor for promoting and monitoring plant growth in smart farming. *Chem. Eng. J.* **2021**, *422*, 129499.

(23) Yin, S.; Ibrahim, H.; Schnable, P. S.; Castellano, M. J.; Dong, L. A Field-Deployable, Wearable Leaf Sensor for Continuous Monitoring of Vapor-Pressure Deficit. *Adv. Mater. Technol.* **2021**, *6* (6), 2001246.

(24) Hossain, N. I.; Tabassum, S. A hybrid multifunctional physicochemical sensor suite for continuous monitoring of crop health. *Sci. Rep.* **2023**, *13* (1), 9848.

(25) Lee, G.; Hossain, O.; Jamalzadegan, S.; Liu, Y.; Wang, H.; Saville, A. C.; Shymanovich, T.; Paul, R.; Rotenberg, D.; Whitfield, A. E.; et al. Abaxial leaf surface-mounted multimodal wearable sensor for continuous plant physiology monitoring. *Sci. Adv.* **2023**, *9* (15), eade2232.

(26) Wang, L.; Zhang, Z.; Cao, J.; Zheng, W.; Zhao, Q.; Chen, W.; Xu, X.; Luo, X.; Liu, Q.; Liu, X.; et al. Low Hysteresis and Fatigue-Resistant Polyvinyl Alcohol/Activated Charcoal Hydrogel Strain Sensor for Long-Term Stable Plant Growth Monitoring. *Polymers* **2022**, *15* (1), 90.

(27) Zhang, C.; Zhang, C.; Wu, X.; Ping, J.; Ying, Y. An integrated and robust plant pulse monitoring system based on biomimetic wearable sensor. *npj Flex. Electron.* **2022**, *6* (1), 43.

(28) Tang, W.; Yan, T.; Ping, J.; Wu, J.; Ying, Y. Rapid Fabrication of Flexible and Stretchable Strain Sensor by Chitosan-Based Water Ink for Plants Growth Monitoring. *Adv. Mater. Technol.* **2017**, *2* (7), 1700021.

(29) Tang, W.; Yan, T.; Wang, F.; Yang, J.; Wu, J.; Wang, J.; Yue, T.; Li, Z. Rapid fabrication of wearable carbon nanotube/graphite strain sensor for real-time monitoring of plant growth. *Carbon* **2019**, *147*, 295-302.

(30) Lee, H. J.; Joyce, R.; Lee, J. Liquid Polymer/Metallic Salt-Based Stretchable Strain Sensor to Evaluate Fruit Growth. *ACS Appl. Mater. Interfaces* **2022**, *14* (4), 5983-5994.

(31) Verma, R. P.; Sahu, P. S.; Dabhade, A.; Saha, B. IoT-Enabled Stretchable Piezoresistive Sensor for Real-Time Monitoring of Fruit Growth and Human Physiology. *ACS Appl. Nano Mater.* **2024**, *7* (7), 6969-6982.

(32) Lo Presti, D.; Massaroni, C.; Bianchi, D.; Tocco, J. D.; Cimini, S.; Caponero, M. A.; Gizzi, A.; De Gara, L.; Cinti, S.; Schena, E. A Wearable Flower-Shaped Sensor Based on Fiber Bragg Grating Technology for In-Vivo Plant Growth Monitoring. *IEEE Sens. J.* **2023**, *23* (8), 8416-8425.

(33) Xu, K.; Lu, Y.; Honda, S.; Arie, T.; Akita, S.; Takei, K. Highly stable kirigami-structured stretchable strain sensors for perdurable wearable electronics. *J. Mater. Chem. C* **2019**, *7* (31), 9609-9617.

(34) Yong, K.; De, S.; Hsieh, E. Y.; Leem, J.; Aluru, N. R.; Nam, S. Kirigami-inspired strain-insensitive sensors based on atomically-thin materials. *Mater. Today* **2020**, *34*, 58-65.

(35) Kim, Y.-G.; Song, J.-H.; Hong, S.; Ahn, S.-H. Piezoelectric strain sensor with high sensitivity and high stretchability based on kirigami design cutting. *npj Flex. Electron.* **2022**, *6* (1), 52.

(36) Xuan, Y.; Hara, H.; Honda, S.; Li, Y.; Fujita, Y.; Arie, T.; Akita, S.; Takei, K. Wireless, minimized, stretchable, and breathable electrocardiogram sensor system. *Appl. Phys. Rev.* **2022**, *9* (1), 011425.

(37) Li, Y.; Nakamura, H.; Lee, D. H.; Qin, Y.; Xuan, Y.; Takei, K. Temperature Coefficient of Resistance of Transferred Laser-Induced Graphene. *ACS Appl. Electron. Mater.* **2024**, *6* (6), 4630-4634.

(38) Lee, T.-I.; Kim, M. S.; Kim, T.-S. Contact-free thermal expansion measurement of very soft elastomers using digital image correlation. *Polym. Test.* **2016**, *51*, 181-189.

(39) Wu, X.; Han, Y.; Zhang, X.; Lu, C. Highly Sensitive, Stretchable, and Wash-Durable Strain Sensor Based on Ultrathin Conductive Layer@Polyurethane Yarn for Tiny Motion Monitoring. *ACS Appl. Mater. Interfaces* **2016**, *8* (15), 9936-9945.

(40) Duan, L.; D'Hooge, D. R.; Cardon, L. Recent progress on flexible and stretchable piezoresistive strain sensors: From design to application. *Prog. Mater. Sci.* **2020**, *114*, 100617.

(41) Hardie, M. Review of Novel and Emerging Proximal Soil Moisture Sensors for Use in Agriculture. *Sensors* **2020**, *20* (23), 6934.

(42) Faqir, Y.; Qayoom, A.; Erasmus, E.; Schutte-Smith, M.; Visser, H. G. A review on the application of advanced soil and plant sensors in the agriculture sector. *Comput. Electron. Agric.* **2024**, *226*, 109385.

(43) Eldeeb, M. A.; Dhamu, V. N.; Paul, A.; Muthukumar, S.; Prasad, S. Espial: Electrochemical Soil pH Sensor for In Situ Real-Time Monitoring. *Micromachines* **2023**, *14* (12), 2188.

(44) Li, Y.; Mao, Y.; Xiao, C.; Xu, X.; Li, X. Flexible pH sensor based on a conductive PANI membrane for pH monitoring. *RSC Adv.* **2019**, *10* (1), 21-28.

(45) Honda, S.; Shiomi, M.; Yamaguchi, T.; Fujita, Y.; Arie, T.; Akita, S.; Takei, K. Detachable Flexible ISFET-Based pH Sensor Array with a Flexible Connector. *Adv. Electron. Mater.* **2020**, *6* (10).

(46) Korent, A.; Žagar Soderžnik, K.; Šturm, S.; Žužek Rožman, K. A Correlative Study of Polyaniline Electropolymerization and its Electrochromic Behavior. *J. Electrochem. Soc.* **2020**, *167* (10), 106504.

(47) Nyein, H. Y.; Gao, W.; Shahpar, Z.; Emaminejad, S.; Challa, S.; Chen, K.; Fahad, H. M.; Tai, L. C.; Ota, H.; Davis, R. W.; et al. A Wearable Electrochemical Platform for Noninvasive Simultaneous Monitoring of Ca(2+) and pH. *ACS Nano* **2016**, *10* (7), 7216-7224.

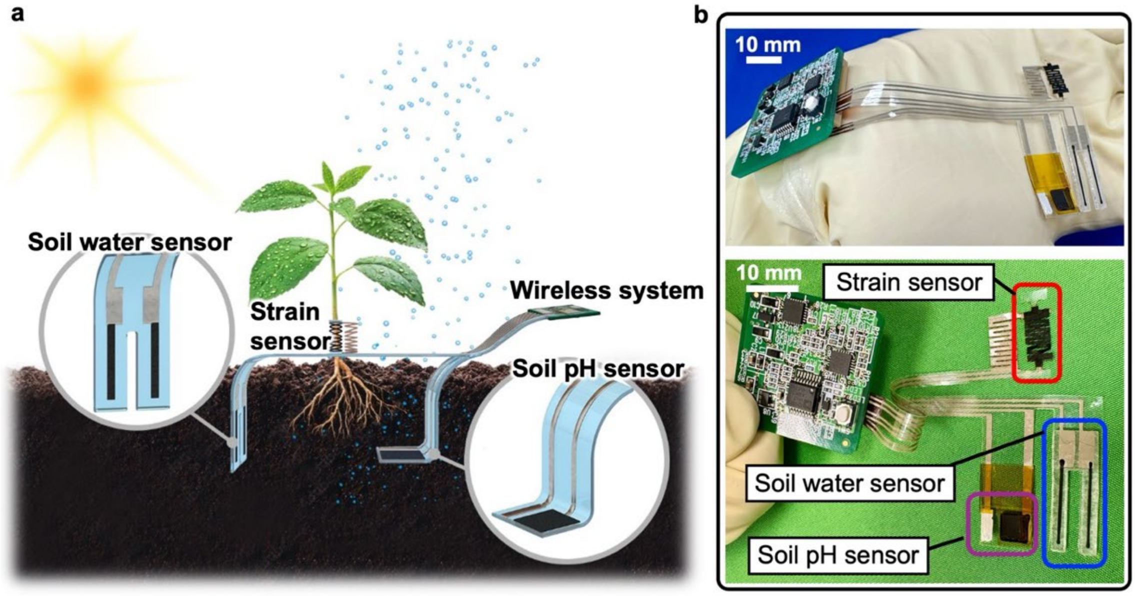

Figure 1. Multimodal flexible sensor sheet. (a) Concept of the sensor system. (b) Photos of sensor sheet.

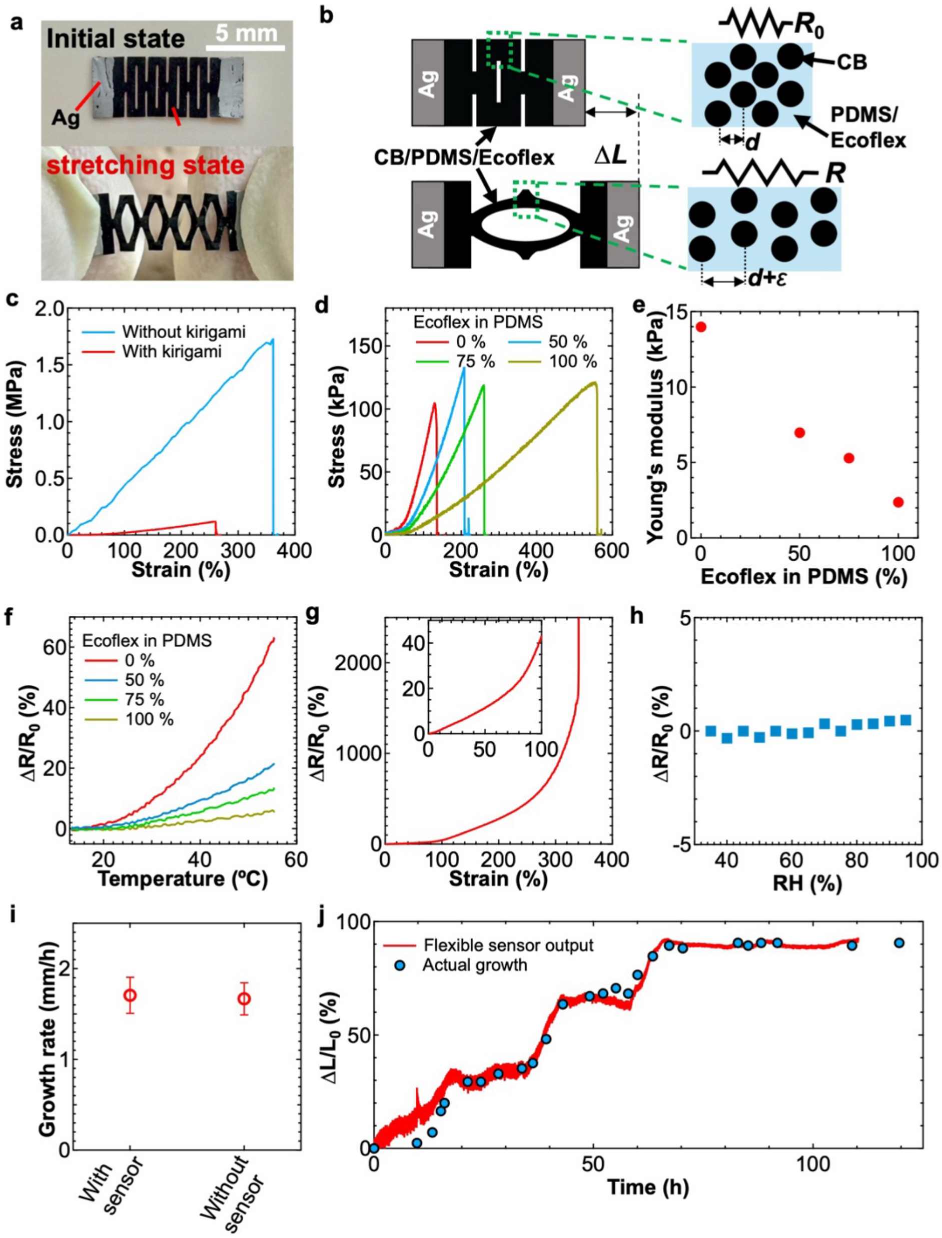

Figure 2. Flexible strain sensor for stem growth monitoring. (a) Photo of the strain sensor. (b) Sensing mechanism of the kirigami-based strain sensor. (c) Stress-strain curves with and without the kirigami structure. (d) Stress-strain curves at different Ecoflex composite ratios in PDMS. (e) Young's modulus at different Ecoflex composite ratios in PDMS extracted from (d). (f) Resistance change ratio as a function of temperature at different Ecoflex composite ratios in PDMS. (g) Resistance change ratio as a function of the applied stretching strain (inset: enlarged plots focusing on strain below 100%). (h) Humidity dependence of the strain sensor. (i) Stem growth rate with and without the sensor (N=6). (j) Real-time growth length monitoring.

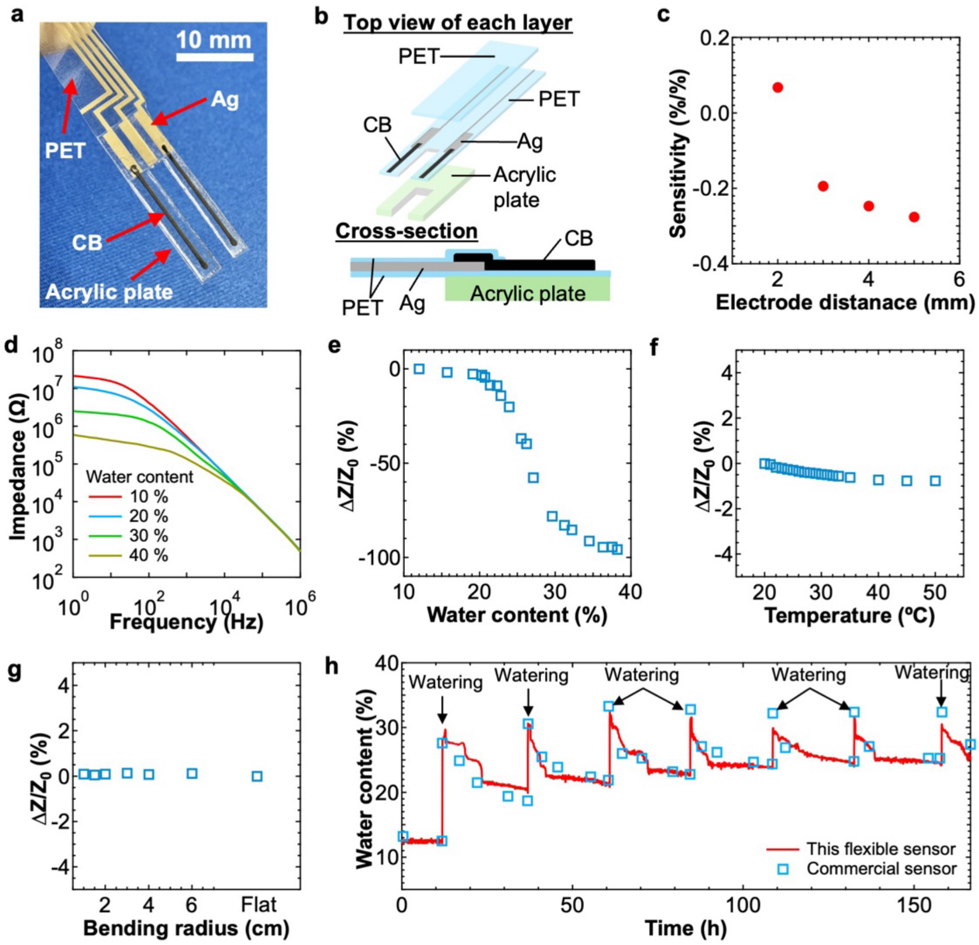

Figure 3. Impedance-based soil water sensor. (a) Photo of the soil water sensor. (b) Schematic image of the sensor with detailed materials. (c) Sensor sensitivity at different electrode distances. (d) Impedance characteristics at different water content. (e) Impedance change ratio as a function of water content in soil at 1 kHz. (f) Temperature dependence of the sensor impedance at 1 kHz. (g) Impedance change ratio at different bending radii at 1 kHz. (h) Time-series real-time water content monitoring using the developed sensor and a commercial sensor.

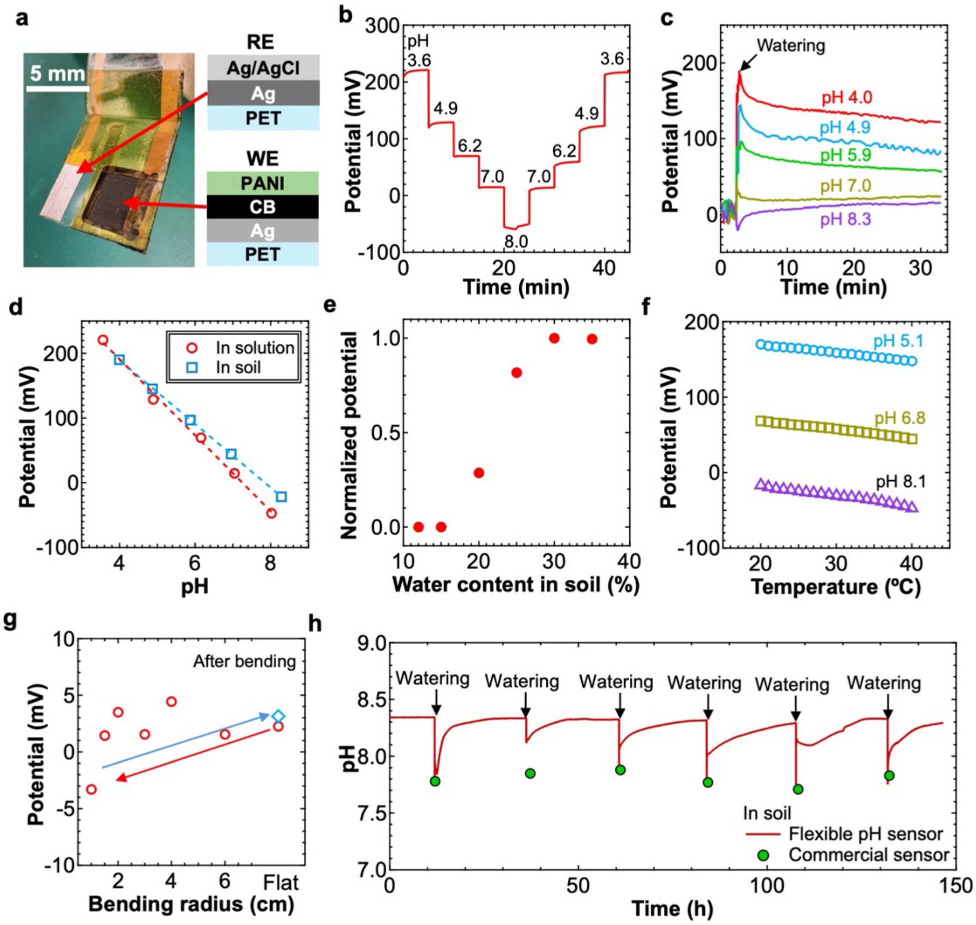

Figure 4. Flexible pH sensor. (a) Photo and schematic image of the pH sensor. Sensor outputs at different pH solutions in (b) solution and (c) soil. (d) Potential change at varied pH in solution and soil. (e) Normalized potential change at different water content in soil. (f) Sensor output as a function of temperature at various pH solution. (g) Sensor output under bending of the sensor. (h) Time-series pH monitoring through multiple irrigation events.

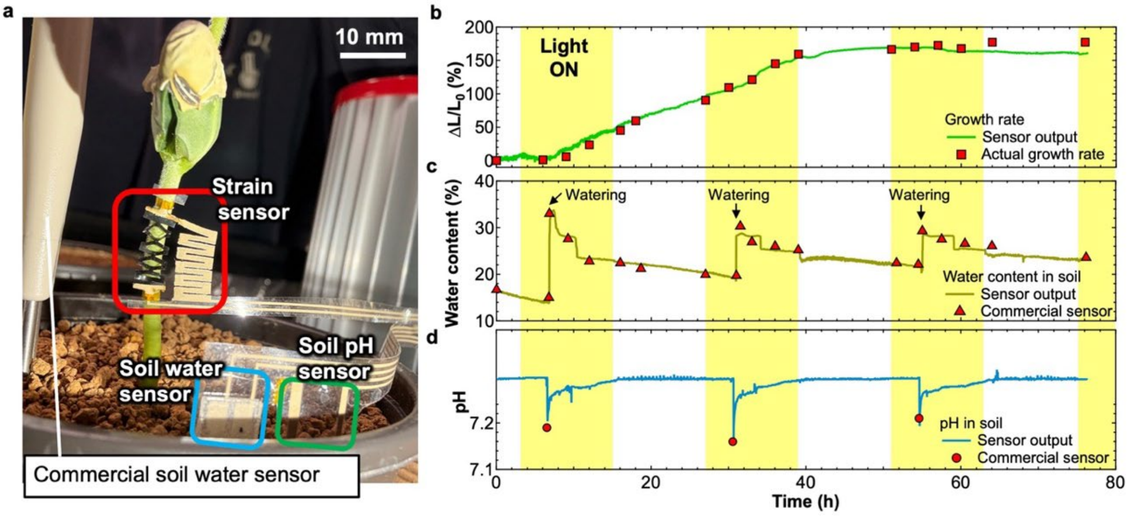

Figure 5. Real-time monitoring of multiple plant conditions. (a) Photo of the experimental setup. Simultaneous time-series sensor outputs of the (b) stem growth, (c) water content in the soil, and (d) pH of the soil water.

ToC